IL NUOVO CIMENTO Vol. 27 C, N. 5 Settembre-Ottobre 2004
DOI 10.1393/ncc/i2005-10015-7

Experimental investigation of magnetohydrodynamic instabilities in a Magneto-Plasma-Dynamic thruster

M. Zuin(1)(2), M. Agostini(1), R. Cavazzana(1), E. Martines(1), P. Scarin(1)
G. Serianni(1), V. Antoni(1)(2), M. Bagatin(1)(2), M. Andrenucci(3)(4)
F. Paganucci(3)(4), P. Rossetti(3)(4) and M. Signori(3)(4)

(1) *Consorzio RFX, Associazione EURATOM-ENEA sulla fusione corso Stati Uniti 4, 35127 Padova, Italy*
(2) *INFM, Unità di Padova - Padova, Italy*
(3) *Dipartimento di Ingegneria Aerospaziale, Università di Pisa - Pisa, Italy*
(4) *Centrospazio - Via A. Gherardesca 5, 56014 Pisa, Italy*

(ricevuto il 20 Gennaio 2005)

Summary. — An extensive experimental investigation has been carried out in order to understand the role of magnetohydrodynamic (MHD) instabilities on the reduced performance of Magneto-Plasma-Dynamic (MPD) thrusters when operating at high current. MPDs are electromagnetic plasma accelerators, currently under investigation as a possible, high-power electric propulsion option for primary space missions, whose thrust efficiency is limited by the onset of critical regimes observed when the current rises beyond a threshold value. Recently, it has been found (Zuin M. *et al.*, *Phys. Rev. Lett.*, **95** (2004) 225003) that in these devices large-scale MHD helical kink mode instabilities develop, with $m/n = 1/1$ azimuthal and axial periodicity, and that the critical current condition is well described by the Kruskal-Shafranov criterion. In this paper the spatial structure of the kink has been reconstructed by magnetic and electrostatic probes and the results of two photomultiplier arrays, 16 channels each, collecting total radiation in the range 350–850 nm, confirm the helical structure of a kink with nonuniform pitch.

PACS 52.75.Di – Ion and plasma propulsion.
PACS 52.35.Py – Macroinstabilities (hydromagnetic, e.g., kink, fire-hose, mirror, ballooning, tearing, trapped-particle, flute, Rayleigh-Taylor, etc.).
PACS 52.70.Ds – Electric and magnetic measurements.

1. – Introduction

Magneto-Plasma-Dynamic (MPD) thrusters, also known as Lorentz force accelerators, are space propulsion devices, where the thrust is produced by the interaction between a high-current discharge, formed in a plasma channel between an anode and a cathode, and

the self-induced (and/or externally applied) magnetic field. By this way, high exhaust velocities of the propellant gas particles can be reached (> 50 km/s), much larger than those attainable with conventional chemical rockets, at thrust densities up to $10^5\,\mathrm{N/m^2}$ higher than those produced by other kinds of electric propulsion devices [1]. Since its invention in 1963 the MPD has potentially had a unique place among all the different electric thrusters in its ability to process megawatts of electrical power in a small, simple, compact device. Currently the major limit on the use of MPD thrusters in real space missions is their low efficiency, which has a maximum in the 20–40% range, while thrust efficiencies higher than 50% are required to make them preferable to chemical or other electric options. In particular, MPDs efficiency is normally observed to degrade above a current threshold condition, whose value depends on the mass flow rate, thruster geometry and applied magnetic field. When this threshold value is reached a variety of disturbing phenomena, including severe fluctuations of the terminal voltage and increased erosion, have usually been observed. The condition at which this unstable discharge behaviour occurs is usually referred to as the *onset*. Simultaneously, the anode losses tend to increase, thus leading to a strong decrease of the efficiency. This transition from *standard* to the so-called *critical* regime is usually characterized by a transition from a uniform current attachment to a spot attachment mode with very high localized current densities on both the anode and the cathode. The voltage fluctuations, depending on operating conditions, can vary on different time scales, ranging from tens of kilohertz to several megahertz [2,3]. A number of theories have been put forward to explain the onset phenomena and to understand the origin of the performance degradation, and in particular to clarify the role played by plasma instabilities. Most of the studies have been concentrated on MPDs with no applied magnetic field, in the so-called self-field MPD configuration.

Theoretical and experimental efforts have been dedicated by some authors [4,5] to the investigation of plasma microinstabilities (in the form of lower hybrid instabilities) as responsible for the enhanced collisionality and anomalous resistivity, which should convert much of the energy deposited in the plasma column into thermal motion, excitation or other energy forms not recoverable for the acceleration process. More recently, an experimental study of the plasma properties near the anode of high-power pulsed MPD has shown a transition of the current collection from a diffuse, low-voltage and low-noise mode to one of high voltage, high noise, and spotty current attachment [3]. The spot mode is suspected to provide an explanation for the anode fall, and the consequent power losses.

Other authors [2] thought that only macroscopic phenomena could induce such a drastic transition as that associated with the *onset* and, in particular, a type of space-charge instability was deemed to play an important role in producing current chopping and onset phenomena.

The plume of applied field devices has been investigated by Hatakeyama *et al.* [6] and more recently by Amagishi *et al.* [7], in order to study the conversion from magnetohydrodynamic (MHD) modes to shear and compressional Alfvén waves, but the attention of these studies was not focused on the thruster performance and no relation with power losses has been proposed.

In a paper by Fruchtman [8] the efficiency limits of self-field and applied-field MPD thrusters have been analyzed. In this analysis, to simplify the analytical treatment, an approximation is introduced by considering the applied and self-induced magnetic fields as parallel. The loss of efficiency is suggested to be due to a nonoptimized use of the electromagnetic energy converted into thermal energy.

Despite the long series of efforts, only a few of which have been recalled here, the origin

of the plasma phenomena regulating the thruster performance is still a matter of debate. In particular, no theory has proved conclusive in explaining the behaviour in detail or in prompting ways to control or postpone the detrimental effects associated with the onset.

More recently we proposed a novel interpretation of the instabilities developing in the plasma produced by applied field MPDs in terms of MHD helical kink mode, and good agreement was found with the Kruskal-Shafranov criterion for a cylindrical plasma column [9]. In this paper new detailed experimental results are discussed, giving deeper information on the geometrical structure of the observed plasma instabilities, shown to be helical kink modes with nonuniform pitch.

The validity of the approximation introduced in ref. [8] will be discussed and in particular the central role played by the magnetic topology of the MPDs on the presence of the critical operating regimes will be emphasized.

The paper is organized as follows: sect. **2** is dedicated to the description of the experimental equipment, in sect. **3** the properties of plasma fluctuations are analyzed. Section **4** is devoted to the discussion of the experimental results and to the comparison with theoretical predictions for the MHD instabilities in a plasma column.

2. – The experimental equipment

2˙1. *The system.* – The MPD thruster object of our investigation is named Hybrid Plasma Thruster (HPT) a schematic of which is shown in fig. 1. The HPT is an axisymmetric MPD thruster which can operate in both self-field and in applied-field configurations, as an axial magnetic field on the thruster axis can be induced by means of an external solenoid. A natural cylindrical coordinate system (r, θ, z) is used and the z-axis is measured from the thruster outlet, taken to point towards the thruster plume (see fig. 1).

The anode consists of eight copper straps which collect most of the current, each 20 mm wide, equally spaced in the azimuthal direction, shaped as shown in fig. 1. This shape is intended to have strap surfaces parallel to the local externally applied magnetic-field lines, so that no direct magnetic link is obtained between anode and cathode, as schematized in fig. 1.

The system is bounded by a copper cylinder (200 mm diameter) electrically connected to the anode straps.

The thruster has a central hollow multichannel cathode, which consists of 19 copper tubes with external diameter of 8.5 mm and thickness of 0.5 mm; they are housed inside a holder tube whose external diameter and thickness are respectively 44 mm and 1.3 mm. The total cross-section area useful for the gas passage is about 1100 mm^2.

A multichannel cathode has been adopted because this kind of solution is known to exhibit a lower erosion rate, an important aspect for steady and quasi-steady MPD thrusters application, and a larger operating range in terms of mass flow rate and current values than those obtainable by more conventional configurations like rod or single-channel cathode.

An aluminum cylinder (150 mm diameter, 100 mm length, 5 mm thickness), electrically insulated from all the electrodes and mounted coaxially to the thruster, surrounds the anode straps acting as a flux conserver for the plasma column (see fig. 1).

The electric power to the HPT is supplied by a Pulse Forming Network (PFN), which can be configurated to supply quasi-steady current pulses (I_{tot}) lasting 2.5 ms or 5 ms.

The propellant feeding system is based on fast acting solenoid valves, which provide gas pulses with a long plateau after few milliseconds from valve activation, which pre-

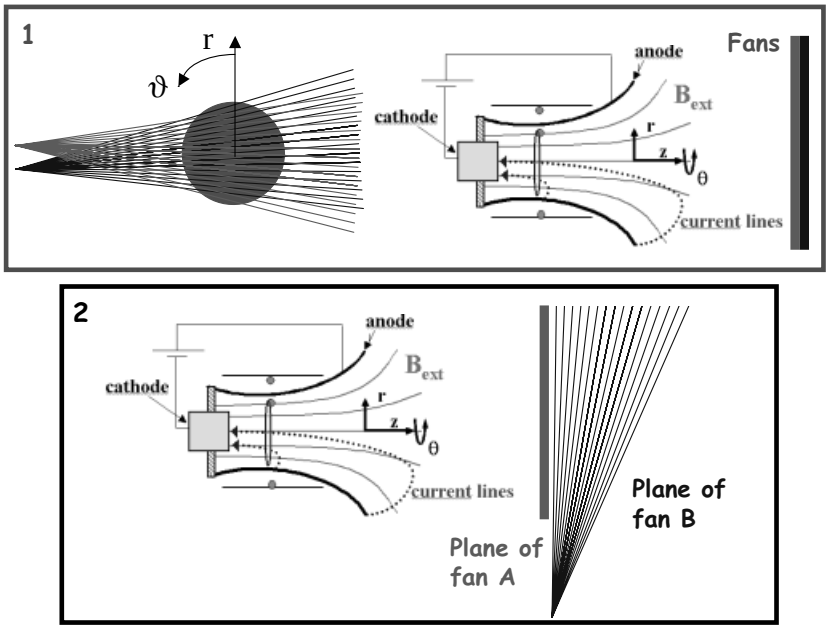

Fig. 1. – Schematic of the HPT and of optical diagnostic set-up, showing shape of the anode straps, external magnetic-field lines, external solenoid, two examples of possible current lines and the fans distribution of the otpic probes.

cedes the electric discharge. The device is provided with two gas-feeding systems, one for the central cathode and the other for eight peripheral injectors equally spaced in the azimuthal direction, located between the anode straps and the external cylinder. The discharge takes place at $t = 0$, when a steady-state mass flow rate is reached. The main propellant used for the experiments described in this paper is argon at a mass flow rate of 660 mg/s. The mass flow is distributed in the ratio of 10:1 between the central and peripheral valves, respectively. Mass flow rate uncertainty is within 5% of the measurement.

A quasi-steady magnetic field (B_{ext}) up to 100 mT on the thruster axis can be induced. A laboratory-made digital device allows to set the solenoid valve activation in order to start the arc discharge when a steady condition is reached for both the applied magnetic field and the mass flow rate. The arc ignition is obtained by closing the main circuit by switching an ignitron on. A voltage of several hundred volts is applied between the central cathode and the anode and the electrical breakdown occurs. The propellant is ionized and begins conducting currents of several hundred amperes in a diffuse plasma arc. During the discharge the applied voltage is normally of the order of some tens of volts.

To avoid anomalous discharges involving the vacuum chamber, the thruster electrodes are floating with respect to the ground and the arc voltage (ΔV) is obtained by measuring the potential of each electrode with respect to the ground by means of two high-voltage probes. The arc voltage is then obtained by subtracting the cathode voltage signal from the anode voltage signal. Typical measured arc current I_{tot} and ΔV signals are shown in fig. 2, while the electrical characteristics (I *vs.* ΔV curves) obtained for three different B_{ext} values can be found in fig. 3. In particular at low B_{ext} values, a clear knee in the

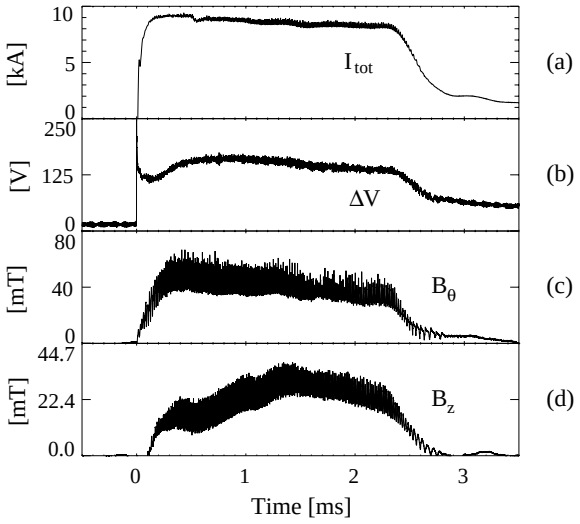

Fig. 2. – Time history of a typical discharge: (a) total current $I_{\rm tot}$, (b) potential difference between anode and cathode ΔV, (c) azimuthal magnetic field B_θ measured at $r = 41$ mm, (d) axial magnetic field B_z measured at $r = 18$ mm. $B_{\rm ext} = 100$ mT and $I_{\rm tot} = 9$ kA.

electrical characteristic is exhibited by the HPT at a current level decreasing with $B_{\rm ext}$. This abrupt change in the electrical characteristic is associated to the transition from *standard* to the so-called *critical* operating regimes, characterized by unstable behaviour and largely increased power losses.

The device is mounted on a thrust stand inside a cylindrical vacuum chamber (length = 3.5 m, radius = 0.6 m), which allows to maintain a back pressure of the order of 10^{-2} Pa during the pulse. The size of the vacuum chamber is generous enough to avoid plasma-wall interactions for the plume of the thruster; this is an important condition, which

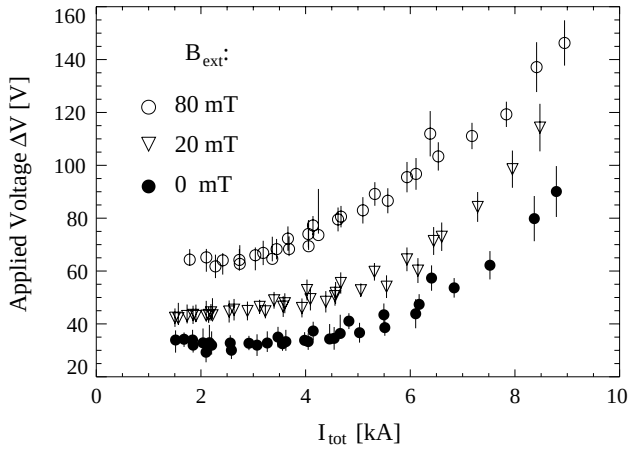

Fig. 3. – Electrical characteristic (ΔV *vs.* $I_{\rm tot}$), of the HPT discharge for different $B_{\rm ext}$ values. Error bars come from averaging over different shots.

validates the hypothesis that the plasma is freely expanding and that boundary effects are not crucial in determining the discharge behaviour.

In the experiments described herein the discharge current $I_{\rm tot}$ has been varied in the range 1.5–9 kA, and an external field $B_{\rm ext}$ from 0 to 100 mT has been applied, so that several critical and non-critical regimes have been explored. The thruster has been operated in power regimes spanning from 45 kW to 1.6 MW. The voltage difference between the anode and the cathode ranges from 30 to 180 V after breakdown, corresponding to a charge of the PFN ranging from about 400 to 1350 V.

3. – The diagnostic setting-up

Different arrays of magnetic, electric and optical probes have been used in order to investigate the space-time properties of the plasma fluctuations in the inter-electrodes and in external regions of the thrusters. The estimated bandwidth for electrostatic and optical measurements is limited to about 500 kHz, whereas for magnetic signals it extends up to ~ 6 MHz. For electrostatic and magnetic sensors, the acquisition sampling frequency was 20 MHz; for optical signals, 10 MHz was adopted.

3˙1. *Magnetic sensors.* – The first system consists of six three-axial magnetic coils housed in quartz tubes, each tube containing two probes spaced by 15 mm. All quartz tubes have been inserted parallel to the main axis, two of them located at $r = 41$ mm, azimuthally spaced by $\pi/4$, the third at $r = 18$ mm. The most inserted sensors have been located in two different axial positions: at $z = -109$ mm, *i.e.* in the point where the vacuum magnetic flux tubes have the minimum diameter, and at $z = 0$ mm (see fig. 1). Each probe consists of three coils wound with 0.2 mm diameter wire on a small parallelepiped-shaped support (7 by 7 by 8 mm).

The second magnetic diagnostic system consists of two azimuthal arrays of equally spaced bi-axial magnetic probes, measuring $\dot{B}_z$ and $\dot{B}_\theta$ mounted on the inner surface of the flux conserver at $z = -150$ mm and $z = -109$ mm.

An additional linear array of equally spaced 21 $\dot{B}$ probes has been used. Each single probe measures one component of the magnetic field fluctuations. They have been disposed in order to measure the azimuthal and axial B-field components alternatively on a radial array, 12 cm long, at $z = 0$.

3˙2. *Electrostatic sensors.* – A circular array of eight equally spaced electrostatic sensors has been used, with 31 mm radius, which has been placed in the same axial positions as the most inserted magnetic probes, *i.e.* at $z = -109$ mm and $z = 0$ mm. Each probe is a tungsten wire, 1 mm radius, 2 mm long, housed in a quartz tube and has been used for floating potential measurements. The floating potential $V_{\rm f}$ is related to the plasma potential $V_{\rm p}$ and to the electron temperature $T_{\rm e}$ by

$$V_{\rm f} = V_{\rm p} - \alpha T_{\rm e}\,, \tag{1}$$

where α is a positive constant [10]. Previous experiments performed in this kind of thruster by means of triple Langmuir probes have shown that electron temperature fluctuations exhibit the same spectral properties as floating potential (and density) fluctuations [11]. As commonly done in other systems [12], temperature fluctuations have been thus neglected in this context, so that floating potential fluctuations are considered as representative of plasma potential fluctuations.

3˙3. *Optical diagnostic.* – An optical diagnostic system has been used to view the thruster plume. The optical system comprises two fans which have been arranged in two different configurations, as shown in fig. 1. In the diagnostic arrangement no. 1, the fans intersect each other at an angle of 7 deg in a plane perpendicular to the thruster plume; this arrangement will make it possible to evaluate the two-dimensional pattern of emitted radiation. Such a work is in progress. With the second arrangement, the simultaneous investigation of emitted radiation can be carried out both on the plane perpendicular to the thruster plume and along the axial direction, though it must be always born in mind that the optical signals are line-integrated. Only results from the second arrangement will be presented in the present paper.

Each fan spans 10 deg and comprises sixteen lines of sight. In the focal region the spacing between adjacent lines of sight is 9 mm and the beams have a diameter of 7 mm. The light is collected by the optics (focal length 85 mm, f-number 11 for fan A and f-number 16 for fan B), located outside the vacuum chamber, after passing through the vacuum window and an attenuating neutral filter (attenuation factor equals to 1000 and 4000 for fan A and B, respectively), and reaches two detectors equipped with a 16 channel photomultiplier array Hamamatsu 5900U-20-L16 each. The current-to-voltage converters developed for this application are based on OP-37 operational amplifiers, configured as transimpedance converters with a gain of 20 mV/μA. At this gain the equivalent noise input level generated by the converter is of the order of the dark current of the PMT sensor and the analog bandwidth is 1.8 MHz. A further gain/buffer stage amplifies the signal by a factor between 2 and 5 [13].

4. – Plasma fluctuation properties

Typical waveforms of the discharge current I_{tot}, the voltage difference between anode and cathode ΔV, the azimuthal magnetic field B_ϑ measured by the insertable probe at $r = 41$ mm and the axial magnetic field B_z at $r = 18$ mm are shown in fig. 2. All the magnetic quantities have been obtained through a numerical integration of the probe signals. Since sampling starts after the externally applied axial field is switched on, the B_z signal does not include such field, which, as already mentioned, is constant throughout the discharge.

The first important feature in fig. 2 is the generation of a large positive B_z of about 25 mT after the start of the plasma current ($t > 0$), the discharge has a paramagnetic behaviour, increasing the externally applied field ($B_{\mathrm{ext}} = 100$ mT in this case). The second important feature is the presence of strong fluctuations on all signals during the discharge. The latter feature is confirmed by the optical signals, an instance of which is presented in fig. 4.

Figure 5 shows the temporal behaviour of four external B_z measurements from the azimuthal array of probes located at $z = -109$ mm and of the inner measurements of B_r, B_ϑ and B_z, together with the eight floating potential signals. A regular oscillation at about 100 kHz can be seen in all signals, both for magnetic and electrostatic measurements. A well-defined phase difference between the probes is observed, implying an azimuthal propagation (rotation) with the same angular velocity for the inner electrostatic array of probes and the external magnetic array.

In fig. 6a the power spectrum of a single floating potential signal measured at $r = 41$ mm in two different positions (at $z = 0$ and $z = -109$ mm) is plotted. Figure 7 displays the power spectrum of the optical signal corresponding to line of sight 12, lying

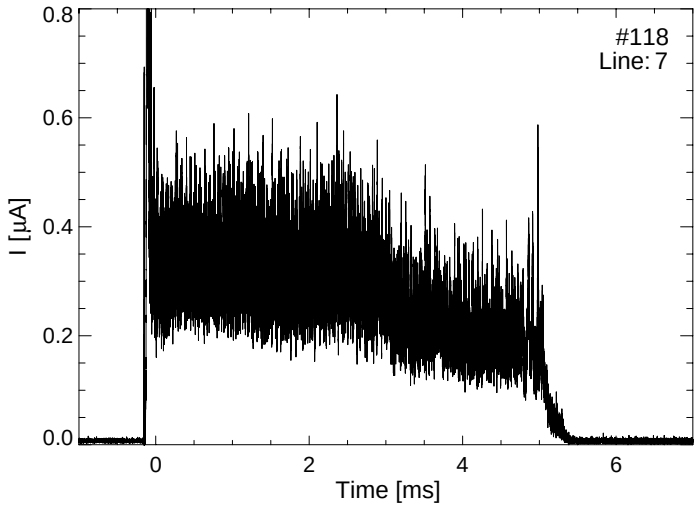

Fig. 4. – Time history of line of sight number 7, in the centre of the fan ($B_{\rm ext}$ = 100 mT, $I_{\rm tot}$ = 9 kA, mass flow rate 120 mg/s).

on the external side of the fan. Figure 6a confirms, in the frequency range explored, the presence of a dominant electrostatic oscillation for the inner ($z = -109$ mm) measurements at about 100 kHz. It is worth to note that the same frequency peak is observed in fig. 6b for the power spectra of a magnetic signal (B_r in this case) taken in the same experimental conditions, and, more important, almost the same frequency is observed

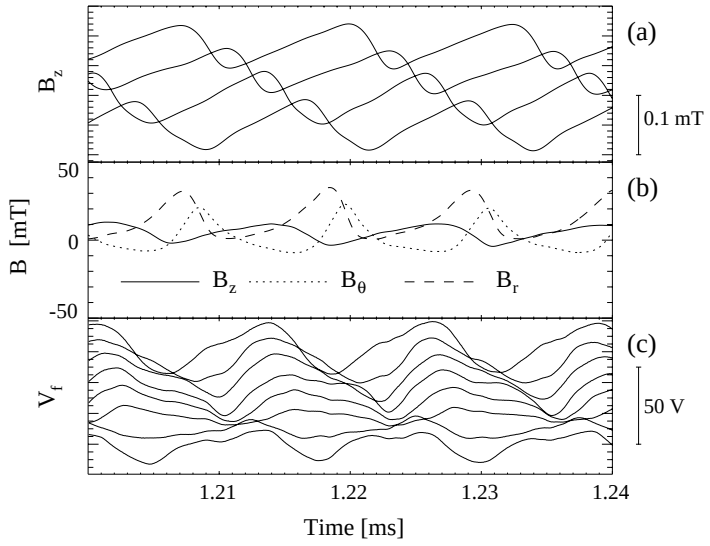

Fig. 5. – Temporal evolution of: (a) 4 B_z signals close to the flux conserver, (the scale refers to one signal, the others having been vertically shifted), (b) B_r, B_θ, B_z measured at r = 18 mm, (c) eight $V_{\rm f}$ signals (vertically shifted). $B_{\rm ext}$ = 100 mT and $I_{\rm tot} \simeq 8$ kA, in this case.

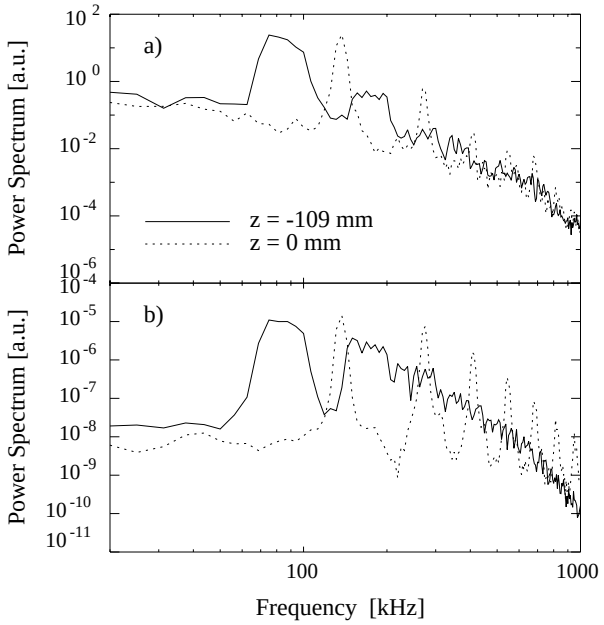

Fig. 6. – Power spectra of (a) floating potential and (b) B_r signal for two different experimental conditions ($B_{\text{ext}} = 100$ mT and $I_{\text{tot}} = 9$ kA, in these cases).

on the signals from measurements at $z = 0$ mm and even in the thruster plume (fig. 7). Higher harmonics can also be observed; their presence seems to be related to a nonsinusoidal behaviour of the signals (see fig. 5). The frequency of the main spectral peak increases almost linearly with the current and is only slightly affected by the application of the external magnetic field.

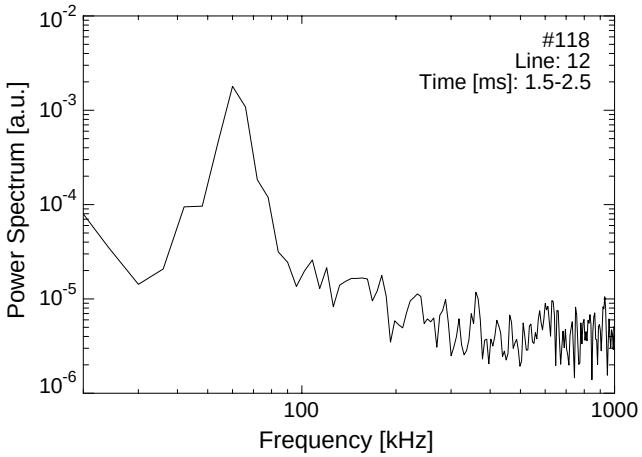

Fig. 7. – Power spectra of optical signal corresponding to line of sight 12 ($B_{\text{ext}} = 100$ mT, $I_{\text{tot}} = 9$ kA.

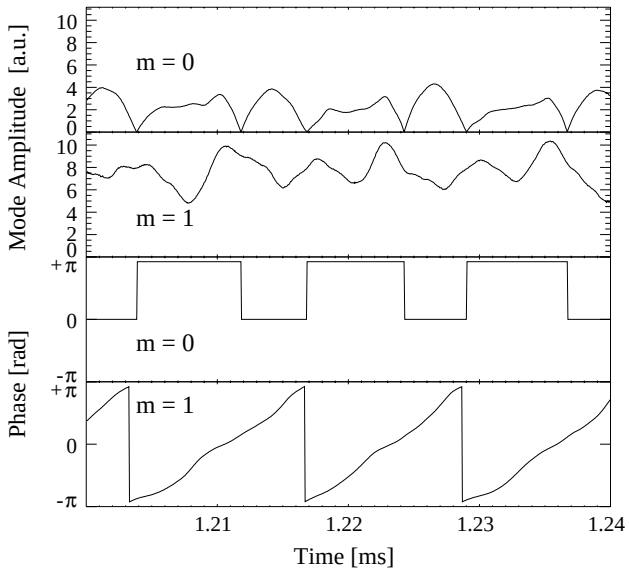

Fig. 8. – Temporal evolution of the amplitude of the $m = 0$ and $m = 1$ azimuthal modes and their phases from electrostatic measurements($B_{\text{ext}} = 100$ mT and $I_{\text{tot}} = 8$ kA, in this case).

A spatial Fourier decomposition technique has been applied to the eight electrostatic signals, belonging to the circular array, to investigate the spatio-temporal pattern of fluctuations, obtaining the time behavior of mode amplitudes and phases. The amplitudes $a_m(t)$ and the phases $\alpha_m(t)$ are related to the measured field $x(t)$ (in this case the floating potential) by

$$x(\vartheta, t) = \sum_{m=0,1\ldots} a_m(t) \cos[m\vartheta + \alpha_m(t)] \,. \tag{2}$$

In practice, amplitudes and phases are computed by applying the Fast Fourier Transform (FFT) algorithm to the 8 electrostatic measurements at each sampling time. Nyquist's sampling theorem restricts the mode number range to $m = 0$–3, while for $m = 4$ only part of the total mode amplitude can be recovered. The typical time evolution for $m = 1$ and $m = 0$ modes amplitude, during the stationary part of the discharge is shown in fig. 8 together with their phases. The largest amplitudes are obtained for the lowest-order modes ($m = 1$ and $m = 0$), which grow few microseconds after $t = 0$ and then oscillate during the plateau phase. Higher-order modes ($m > 1$) normally exhibit almost negligible amplitude. It is found that $m = 1$ is the dominant azimuthal periodicity and the linear dependence of the phase on time confirms the rotation at a frequency of about 100 kHz. The $m = 0$ pulsates almost sinusoidally with the same frequency of the $m = 1$.

Similar results are obtained from the line-of-sight–integrated optical measurements shown in fig. 9, by computing the half sum and the half difference between lines of sight 5 and 14. The specific lines have been chosen as the ones which look more symmetrical with respect to the thruster plume, probably due to some equipment misalignment.

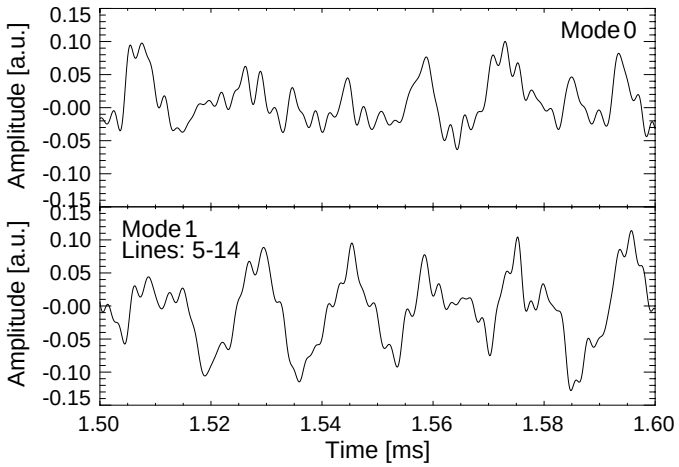

Fig. 9. – Temporal evolution of the amplitudes of the $m = 0$ and $m = 1$ azimuthal modes, as obtained from the optical measurements ($B_{\rm ext} = 100$ mT, $I_{\rm tot} = 9$ kA).

The $m = 1$ mode frequency shows a linear dependence on $I_{\rm tot}$ (ranging from 30 to 100 kHz for $1.5 < I_{\rm tot} < 9$ kA, corresponding to a rotation velocity of about 20 km/s measured at $r = 41$ mm), whereas it has only a weak dependence on $B_{\rm ext}$. The propagation direction changes sign when the external field is reversed and is consistent with that of the $\mathbf{E} \times \mathbf{B}$ drift of the particles.

A comparison of frequency and amplitude measurements performed by means of the external probes with and without the insertion of the internal diagnostic system has shown that its presence does not significantly modify the plasma dynamics.

Figure 10 shows the total energy of the $m = 0, 1$ modes as a function of $I_{\rm tot}$ for the cases with $B_{\rm ext} = 0, 20, 80$ mT. The mode energy is time averaged over 1 ms during the plateau phase. It can be noticed that the time-averaged amplitude of the dominant $m = 1$ mode depends on $I_{\rm tot}$ and $B_{\rm ext}$ values. At the highest current the averaged amplitude of the $m = 0$ mode increases, being comparable to the amplitude of the $m = 1$ mode at low $B_{\rm ext}$ values. As an example, for low $B_{\rm ext}$ values the mode energy is almost zero for $I_{\rm tot} < I_{\rm cr} \simeq 5.5$ kA and the $m = 1$ amplitude jumps to high positive values when the current rises beyond the critical value. At high applied field, $B_{\rm ext} = 80$ mT for the case in fig. 10c, the critical condition appears at lower current, so that the mode amplitude is low only for $I_{\rm tot} \leq 2$ kA, and increases with increasing power.

It is worth to say that very good agreement is found between the change of the slope in the ΔV *vs.* $I_{\rm tot}$ curve, *i.e.* the transition from standard to critical thruster regimes (see fig. 3), and the steep growth of the modes. This is a clear indication that the observed azimuthally rotating low order modes are responsible for the unstable behaviour of MPDs at high current.

Using two axially spaced magnetic probes, the axial structure of the modes has been analyzed, upon evaluating the spectral density $S(k_z,f)$, where k_z is the wave vector in the axial direction and f is the frequency, by means of a two-point statistical technique [14, 15].

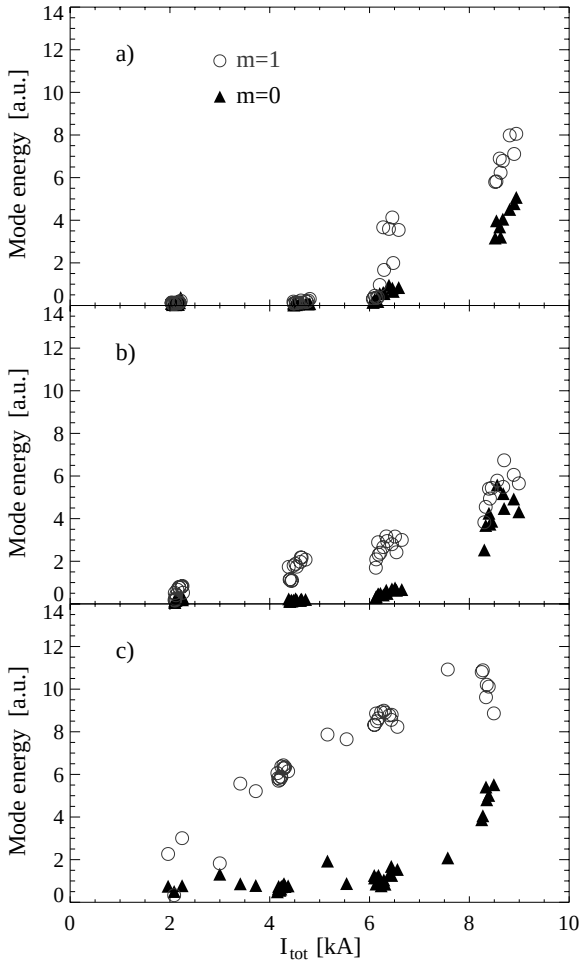

Fig. 10. – Energy of $m = 0$ and $m = 1$ modes, as a function of the $I_{\rm tot}$, averaged over time during the plateau phase (∘) for: a) $B_{\rm ext} = 0$, b) $B_{\rm ext} = 20$ mT, c) $B_{\rm ext} = 80$ mT.

In fig. 11 the spectral density $S(k_z, f)$ obtained at $z = -130, -75, -40$ mm, from magnetic probes measuring $\dot{B}_\theta$, for two different $B_{\rm ext}$ values is shown.

The most prominent feature of the plot is the presence of a relatively sharp peak appearing at the main oscillation frequency of the signals, corresponding to a single discrete wave vector. Values of k_z ranging from 5 to 60 m^{-1} have been obtained, which imply wavelengths λ_z from about 0.1 to 1 m. Measurements in different experimental conditions ($I_{\rm tot}$ and $B_{\rm ext}$) have confirmed the almost linear increase of the frequency with the current (as already mentioned) and have shown that the axial wavelength λ_z, measured close to the cathode (at $z < -100$ mm), tends to increase with $B_{\rm ext}$. Morevover, it is important to notice that at low $B_{\rm ext}$ (left column), the shorter k_z, *i.e.* the larger λ_z, are observed the larger is the distance from the cathode in the axial direction. At high $B_{\rm ext}$ (right column) the dependence on the position appears weaker. The configuration 2 of the optical measurements provided an estimation of the values of λ_z at $z > 0$, which are comparable to those obtained in the inter-electrodes region at $z = -40$ mm.

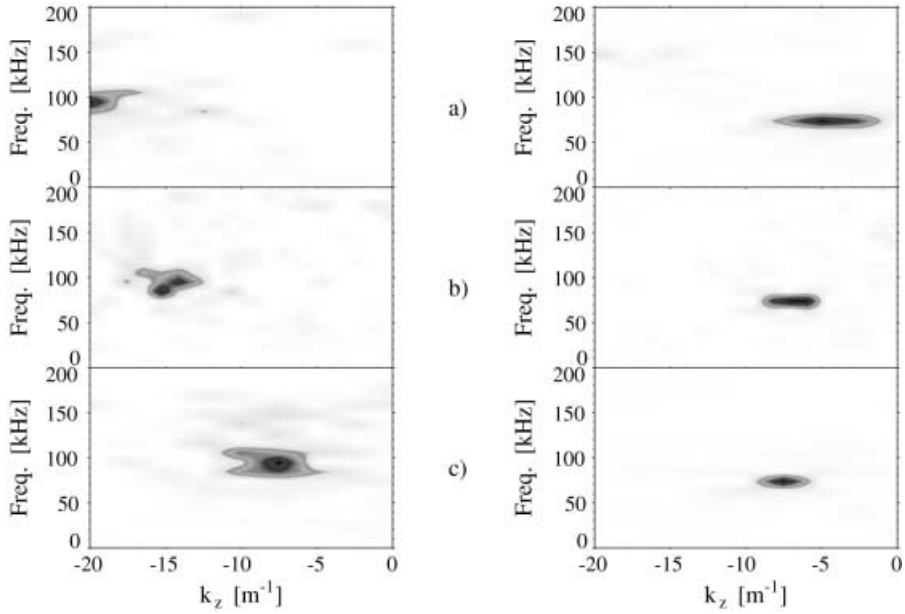

Fig. 11. – Spectral density $S(k_z,\mathrm{f})$ deduced from the signals of two axially spaced magnetic probes, measuring the azimuthal component of the fluctuating magnetic field B_θ at: a) $z = -130$ mm, b) $z = -75$ mm, c) $z = -40$ mm. The left column refers to cases with $B_{\mathrm{ext}} = 20$ mT, while the right column to $B_{\mathrm{ext}} = 80$ mT conditions. $I_{\mathrm{tot}} = 4$ kA in this case.

Optical measurements in high B_{ext} regimes [16] show that the plasma plume extends up to 0.4 m outside from the thruster outlet. Therefore the result of the total axial length of the plasma column L is about 0.6 m, comparable to the averaged axial wavelength measured in the same experimental conditions. As a consequence the mode results in winding once azimuthally for an equivalent $n = 1$ axial periodicity. This result leads to the conclusion that the mode is a $m/n = 1/1$ helical kink mode.

The interpretation of the observed plasma instability in terms of helical kink mode has been recently confirmed by an experimental investigation performed on an MPD thruster, with geometrical properties very close to those of the HPT, by Bonomo *et al.* [17] by means of ultraviolet (UV) imaging techniques. In that experiment the presence of a kink, originating at the cathode, and gradually moving radially towards the edge, while azimuthally rotating is evidenced. It is interesting to note that Bonomo *et al.* observed a deformation of the kink from a well-defined bean-like structure to a more complex one when it axially moves from the cathode to the anode. This behaviour is in good agreement with the one detected in plasma guns by Hsu and Bellan [18], who saw a *mushroom cap* at the kink-end on the open side of their system.

The observation of discrete wavelengths in the axial direction in open systems, where a continuum of wavelengths would be expected, is a rather common feature in plasma physics. Similar results have been found not only in the cited case of the plasma gun for spheromak formation [18], but also in other open devices. The most important example relates to the observation of galactic magnetic writhed jets by Nakamura *et al.* [19], who proposed a possible explanation, suggesting that a local discontinuity on the Alfvén velocity can act as a virtual axial boundary for the system.

5. – Discussion

As we suggested in ref. [9], the magnetic topology of the applied-field MPD thruster, with its combination of applied field, which, at least in the inner part, has a dominant axial component and mostly parallel current, places this system within the wide category of devices generally labeled as screw pinches. Screw pinches can be subjected to current driven large-scale MHD instabilities when some threshold of the ratio between axial current and axial applied magnetic field is exceeded, with effects which range from distortion or changes in the topology of the discharge to its disruption [20].

A peculiar feature of many of such systems is that such MHD instabilities can lead to an amplification of the applied magnetic flux, linked to a spontaneous reorganization of the current density pattern inside the device [21, 22]. This is usually labeled as *dynamo effect*. In particular Taylor conjectured that in a laboratory plasma, characterized by a low β value and finite dissipation $\eta \neq 0$, the time decay of magnetic helicity is longer than the time decay of magnetic energy [23]. As a consequence the plasma is expected to relax to a minimum energy state under the constraint of total constant magnetic helicity. The profiles corresponding to this state are found to be solution of the equation

$$\nabla \times \mathbf{B} = \mu \mathbf{B}\,, \tag{3}$$

where μ is a constant given by $\mu = \mu_0 \mathbf{J} \cdot \mathbf{B}/B^2$. These states are called *force free*, and in cylindrical coordinates it is straightforward to demonstrate that a solution of eq. (3) is $B_\theta(r) = B_0 J_1(\mu r)$, $B_z = B_0 J_0(\mu r)$ and $B_r(r) = 0$, where B_0 is the magnetic field on the axis (r=0) and J_0, J_1 are the Bessel functions of zero and first order, respectively (Bessel Function Model, BFM). The solutions are determined by the value of B_0 which fixes the fields amplitudes and μ which describes the radial dependence.

It is important to note that this approach, which emphasizes the effects of the current component J_z parallel to the applied magnetic field, is substantially different from the ones previously adopted to interpret MPD plasma instabilities. In particular, the purely cross field (radial) component of the plasma current is usually taken into account not only to explain the current driven microinstabilities [4, 5, 24], but also for the analytical derivation of a dispersion relation for macroinstability such as the space-charge instability in unbounded plasmas [2]. These approaches were forced by the choice to concentrate the investigation on the self-field MPD configuration, which is naturally characterized by totally orthogonal plasma current and magnetic-field lines. Our approach will even be different from the one adopted by Fruchtman [8] who dedicated some attention both to the self-field and applied-field configurations, but, to obtain analytically treatable equations, simplified the applied-field MPD magnetic topology by considering the applied magnetic field as parallel to the self-generated one. In the following we will treat the self-field case as a special one of the more general applied-field MPD configurations.

It is well known that in the screw pinch topology a perturbation for the system, characterized by a two-dimensional wave (propagation) vector $\mathbf{k}$, can induce the development of large-scale MHD instability only if the condition $\mathbf{k} \cdot \mathbf{B} = \mathbf{0}$ is satisfied [20]. This can happen only at special surfaces of radius r, where the the safety factor $q(r)$ assumes rational values $q(r) = m/n$, with m and n azimuthal and axial periodicity, respectively. In a screw pinch, magnetic-field lines will have helical geometrical structure, whose pitch is determined by the ratio B_θ/B_z. The stability of the $m/n = 1/1$ kink mode is determined by the Kruskal-Shafranov condition, which requires $q > 1$ at each radius.

In the HPT the situation is more complex than in an ideal screw pinch, due to the

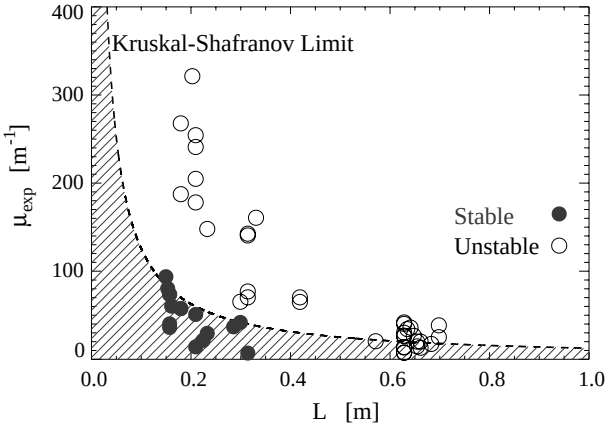

Fig. 12. – Plot of $\mu_{\rm exp}$ as a function of the plasma column length L. Dashed line is the Kruskal-Shafranov limit, which divides stable/unstable regions.

presence of a radial current density, which allows the current to flow from the anode to the cathode. As a consequence, the axial current is not constant along the plasma column, but is a decreasing function of the axial position z. For the present analysis, the axial current $I_{\rm exp}$ at the probe axial position has been directly obtained by measuring B_θ close to the anode and applying Ampere's law, with the assumption of azimuthal symmetry.

In a paramagnetic system the q profile is expected to be a decreasing function of the radius [20], so that the Kruskal-Shafranov criterion [22] prescribes that the q value at the edge of the plasma column must be greater than 1 for the $m/n = 1/1$ stability. This can be recast in terms of the parameter $\mu = \mu_0 I/\Psi$, where I is the plasma current and Ψ is the flux of the externally applied axial magnetic field.

The stability threshold for the $m/n = 1/1$ mode is thus given by $\mu = 4\pi/L$, and the region of stability corresponds to $\mu < 4\pi/L$.

In order to check the applicability of the Kruskal-Shafranov limit to the MPD thruster, we have computed the μ value for different experimental conditions, only for the cases with $B_{\rm ext} > 0$. In such evaluation Ψ is computed by assuming a plasma column radius of 40 mm, and, for the motivations given in the previous section, L is evaluated by the experimental measure of λ_z close to the cathode. The approach for the evaluation of the experimental μ value ($\mu_{\rm exp}$) must be necessarily different from the one adopted for the study of the kink instability in the plasma guns for helicity injection [18], due to the different magnetic topology. In those devices, as already mentioned, a direct linking between the electrodes is established by the magnetic-field lines, so that the total plasma current is taken into account in the evaluation of μ. For the case of the HPT in the formula for $\mu_{\rm exp}$ only the experimental current value $I_{\rm exp}$ must be used, as obtained from the B_θ measurements.

The $\mu_{\rm exp}$ values have been plotted in fig. 12 as a function of the plasma column length L. Stable and unstable cases have been sorted out according to a threshold on the mode energy, namely 10% of the maximum mode energy observed over all the experimental conditions at a given $B_{\rm ext}$ value. The final result is not affected by this choice, due to the fast increase in mode energy observed beyond the stability threshold (see fig. 10). The result shows an excellent agreement with the theoretical Kruskal-Shafranov limit, plotted as a dashed line.

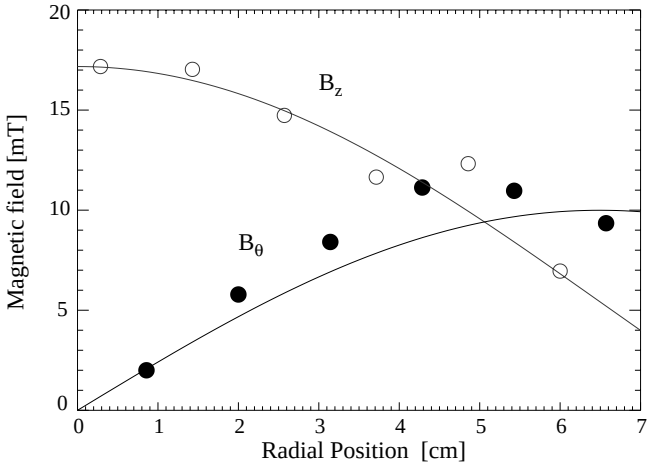

Fig. 13. – Plots showing radial B_z and B_θ profiles, compared with Taylor's solutions, $\mu = 28\,\mathrm{m}^{-1}$.

It is interesting to notice that the best agreement is obtained for the shortest estimated column lengths ($L < 0.4$ m). This feature can again be explained by the strong dependence of B_{ext} on the axial position z for $z > 0$ (see fig. 1). In the anode region, as can be schematically seen in fig. 1, magnetic-field lines generated by the external solenoid are characterized by stronger radial component when moving to $z > 0$ positions. In this condition the schematization of the plasma column in terms of screw pinch is no more valid, because the ratio B_z/B_θ depends on z. In particular, the observed modification of the helical kink structure in proximity of the thruster outlet deriving by the experimental measure of different axial wavelengths at different axial positions can be associated to the strongly tri-dimensional magnetic topology of the applied-field HPT configuration. Magnetic-field lines in the HPT thus result to have a nonuniform pitch.

All these considerations drive to the conclusion that the mode actually is an $m/n = 1/1$ helical kink mode with nonuniform pitch, developing on a $q = 1$ resonant surface.

By means of the radially array of magnetic probes it is further possible to verify this interpretation, by comparing the experimental radial profile of the B_θ and B_z components of the magnetic fields, with those predicted by Taylor.

B_z is evaluated as the sum of the one experimentally measured by the $\dot{B}$ magnetic coils, which is self-produced by the plasma current and the stationary one, induced by the external solenoid. The resulting radial profiles are compared with Taylor state solution in cylindrical geometry. The best fit, shown in fig. 13, is obtained for a μ value of $28\,\mathrm{m}^{-1}$, which corresponds to a pinch parameter $\Theta(\equiv \frac{B_\theta(a)}{\langle B_z \rangle}$, where $\langle .. \rangle$ represents a volume average and $B_\theta(a)$ is the value of the azimuthal magnetic field evaluated at the edge of the plasma column [22]) close to 1, while the experimental μ_{exp} for the case under consideration is about $20\,\mathrm{m}^{-1}$. It is worth to note that some nonperfect agreement is found, but it must however be reminded that the experimental data are taken at $z = 0$, where the $B_r = 0$ hypothesis, which drives to solutions in terms of Bessel functions, is questionable.

We have thus shown that the onset of the critical regimes at high current is related to the generation of large-scale kink modes, which can be therefore considered as the direct cause of the large wasted energy and reduced thruster efficiency at high power.

The process underlying power losses has not yet been clarified and its physical origin

is still object of experimental and theoretical investigation.

At high current regimes it is possible to hypothesize that any distortion of the plasma column induced by the kink can give rise not only to a modification of the magnetic structure, by means of a paramagnetic process, but also to some net components of the Lorentz force ($\mathbf{J}\times\mathbf{B}$) which can be azimuthally and/or radially directed. Any asymmetry in the current distribution would actually drive the system to experience forces whose resultant is not purely axial, giving thus rise to the thrust limitations at high current levels, which are well described in MPD literature (see, for example, ref. [25]).

The helical rotating distortion can be responsible for an increased plasma-wall interaction, in particular in the anode region, so that, though we have not enough experimental evidence to further support this thesis, the kink could be reasonably considered at the origin of the increased anode deterioration, normally observed above the critical condition.

6. – Conclusions

In this paper an experimental investigation by means of magnetic, electrostatic and optic probes in the inner part of a MPD thruster for space propulsion, both with and without the application of an external axial magnetic field, has shown the fundamental role of plasma instability in the power balance of these devices. It has been reinforced the observation that large-scale MHD instabilities develop when some threshold of the ratio between plasma current and applied magnetic field is exceeded. Such MHD instabilities are demonstrated to be at the origin of the large power losses and to cause the transition from standard to critical operating regimes. A solution is thus given to the yet unsolved problem of the origin of the MPD thrusters onset condition, whose appearance had until now prevented the use of this kind of space propulsive systems in real missions. The observed direct link between kink development and power losses is an important issue, whose interest is not related solely to space applications, but more generally regards energy balance in many plasma devices, in particular those for thermonuclear fusion, where the energy confinement is a critical aspect.

* * *

The authors wish to thank V. Cervaro, N. Pomaro, L. Ranzato, M. Recchia and A. Saglia, for their precious support. This work has been granted by Italian Space Agency (ASI).

REFERENCES

[1] Jahn R. G., *Physics of Electric Propulsion*, *McGraw-Hill Series in Missile and Space Technology* (McGraw-Hill Book Company, New York) 1968, p. 239.
[2] Wagner H. P., Kaeppeler H. J. and Auweter-Kurtz M., *J. Phys. D*, **31** (1998) 519.
[3] Diamant K. D., Choueiri E. Y. and Jahn R. G., *J. Propuls. Power*, **14** (1998) 1036.
[4] Choueiri E. Y., *Phys. Plasmas*, **6** (1999) 2290.
[5] Black D. C., Mayo R. M. and Caress R. W., *Phys. Plasmas*, **4** (1997) 3580.
[6] Hatakeyama R., Inutake M. and Akitsu T., *Phys. Rev. Lett.*, **47**, 183 (1981).
[7] Amagishi Y. *et al.*, *J. Phys. Soc. Jpn.*, **71** (2002) 2164.
[8] Fruchtman A., *Phys. Plasmas*, **10** (2003) 2100.
[9] Zuin M., Cavazzana R., Martines E., Serianni G., Antoni V., Bagatin M., Andrenucci M., Paganucci F. and P. Rossetti, *Phys. Rev. Lett.*, **95** (2004) 225003.
[10] Stangeby P. C., *Plasma Physics Series*, in *The Plasma Boundary of Magnetic Fusion Devices* (Institute of Physics, Bristol and Philadelphia) 2000.

[11] Serianni G. *et al.*, *27th International Electric Propulsion Conference, Pasadena, CA, 2001* (Electric Rocket Propulsion Society, Fairview Park, OH, USA, 2001) IEPC-01-135.
[12] Hidalgo C., *Plasma Phys. Control. Fusion*, **37** (1995) A53.
[13] Cavazzana R. *et al.*, *Rev. Sci. Instrum.*, **75** (2004) 4152.
[14] Beall J. M., Kim Y. C. and Powers E. J., *J. Appl. Phys.*, **53** (1982) 3933.
[15] Levinson S. J., Beall J. M., Powers E. J. and Bengston R. D., *Nucl. Fusion*, **24** (1984) 527.
[16] Andrenucci M. *et al.*, *Proceedings of 28th International Electric Propulsion Conference, 2003, Toulouse, France* (CNES, Toulouse, 2003) IEPC-03-0301.
[17] Bonomo F., Franz P., Spizzo G., Marrelli L., Martin P., Paganucci F., Rossetti P. and Andrenucci M., *12th International Congress on Plasma Physics, Nice, France 2004*.
[18] Hsu S. C. and Bellan P. M., *Phys. Rev. Lett.*, **90** (2003) 215002.
[19] Nakamura M., Uchida Y. and Hirose S., *New Astron.*, **6** (2001) 61.
[20] Freidberg J. P., *Ideal Magneto-Hydro-Dynamics* (Plenum Press, New York) 1987.
[21] Verhage A. J. L., Furzer A. S. and Robinson D. C., *Nucl. Fusion*, **18** (1978) 457.
[22] Ortolani S. and Schnack D. D., *Magnetohydrodynamics of Plasma Relaxation* (World Scientific, Singapore) 1993.
[23] Taylor J. B., *Rev. Mod. Phys.*, **58** (1986) 741.
[24] Tilley D. L., Choueiri E., Kelly A. J. and Jahn R. G., *J. Propuls. Power*, **12** (1996) 381.
[25] Paganucci F. *et al.*, *Proceedings of the 27th International Electric Propulsion Conference, Pasadena, CA, 2001* (Electric Rocket Propulsion Society, Fairview Park, OH, USA, 2001) IEPC-01-132.